


**Magnonic activity of ferromagnetic nanocylinders**Mingming Yang,<sup>1,2</sup> Binghui Yin,<sup>1,2</sup> Zhisheng Li,<sup>1,2</sup> Xiaoyan Zeng,<sup>3</sup> and Ming Yan<sup>1,2,\*</sup><sup>1</sup>*Department of Physics, Shanghai University, Shanghai 200444, China*<sup>2</sup>*Shanghai Key Laboratory of High Temperature Superconductors, Shanghai 200444, China*<sup>3</sup>*Department of Mathematics, Shanghai University, Shanghai 200444, China* (Received 25 October 2020; revised 18 February 2021; accepted 19 February 2021; published 2 March 2021)

The optical activity refers to the rotation of the vibration plane of linearly polarized light traversing certain substances. Here we report an analogous phenomenon for spin waves (SWs) in cylindrical nanowires, whose azimuthal distribution undergoes a continuous rotation as traveling along the wire. This effect, in line with the Fresnel model of the optical activity, is attributed to different propagating speeds of two circular states (left and right handed) composing the SW modes. The SW circular birefringence observed here originates from the overall curvilinear shape of the waveguide. Moreover, the fact that an external field is able to alter the rotatory power of the nanowires is reminiscent of the Faraday magneto-optical effect.

DOI: [10.1103/PhysRevB.103.094404](https://doi.org/10.1103/PhysRevB.103.094404)**I. INTRODUCTION**

The optical activity, i.e., the rotation of the polarization of light caused by the propagation medium, is a remarkable physical effect with far-reaching implications in chemistry and biology [1]. It was first discovered in 1811 by Arago in a quartz crystal and then by Biot in the vaporous or liquid form of organic substances. These optically active materials were found to be either left handed (*l* rotatory) or right handed (*d* rotatory). Later on, Herschel disclosed two types of crystallographic structure of quartz that accounted for the *l* and *d* rotations, respectively. Those two crystal forms, being exactly the mirror image of each other, are called enantiomorphs. In 1848, Pasteur discovered the existence of the so-called optical stereoisomers, which are single molecules that differ in their stereostructures although having the same chemical formula [2]. This finding laid the foundation for the development of stereochemistry and aroused interest in searching for the origin of the chirality in chemistry and biology [3,4].

From a physical point of view, the optical activity is a wave effect intimately associated with chirality. In this paper, we present a similar phenomenon for spin waves (SWs), the collective motion of magnetic moments in magnetically ordered systems. In the last several decades, the SW in magnetic nanostructures has drawn a lot of attention in spintronics [5–9], since it represents a potential energy-efficient carrier of information [10–13]. Previous study has indicated that the geometrical shape of the magnetic sample can have significant influence on spin dynamics [14–50]. A particularly striking effect is the dynamic chiral-symmetry breaking occurring in cylindrical geometry, manifesting in the asymmetric domain-wall motion [18] and SW propagation [21,23] in ferromagnetic nanotubes. Recently, magnetic nanocylinders were proposed to serve as waveguides allowing the

propagation of twisted SW beams carrying orbital angular momentum [35,43]. In this work, we show that the curvilinear shape of nanocylinders leads to a SW effect mimicking the optical activity. In micromagnetic simulations, monochromatic SW modes with nonuniform azimuthal distribution of amplitude were excited in axially magnetized nanocylinders (either hollow or solid). Such a mode, in each cross section of the wire, forms a pattern of a circular standing wave, while the azimuthal locations of the (anti)nodes change continuously during its propagation. This SW circumvolution can be well explained by using the Fresnel model for the description of the optical activity, attributing the rotation of polarization to different propagating speeds of two circular components ( $\mathcal{R}$  and  $\mathcal{L}$  states) that superpose to form the linearly polarized light beam. In our case, the aforementioned SW modes can also be decomposed into an  $\mathcal{R}$  and an  $\mathcal{L}$  state, which possess different dispersion relations and thus propagating speeds. We argue that this SW circular birefringence has a purely geometrical origin, resulting from the influence of the sample curvature on the dipolar interaction partially governing the spin dynamics. In fact, the  $\mathcal{R}$  and  $\mathcal{L}$  states excited separately in simulations yield dispersion relations coinciding with those extracted from the Fresnel model. The rotatory power of the nanowire, depending upon the SW dispersion, can be effectively modulated by applying an external magnetic field, making a formal analogy to the Faraday magneto-optical effect.

**II. SIMULATION METHODS AND RESULTS**

Magnetization dynamics in mesoscopic scale can be described by the Landau-Lifshitz-Gilbert (LLG) equation given by

$$\frac{d\vec{m}}{dt} = \gamma \vec{H}_{\text{eff}} \times \vec{m} + \frac{\alpha}{M_s} \left[ \vec{m} \times \frac{d\vec{m}}{dt} \right], \quad (1)$$

\*Corresponding author: myan@shu.edu.cn

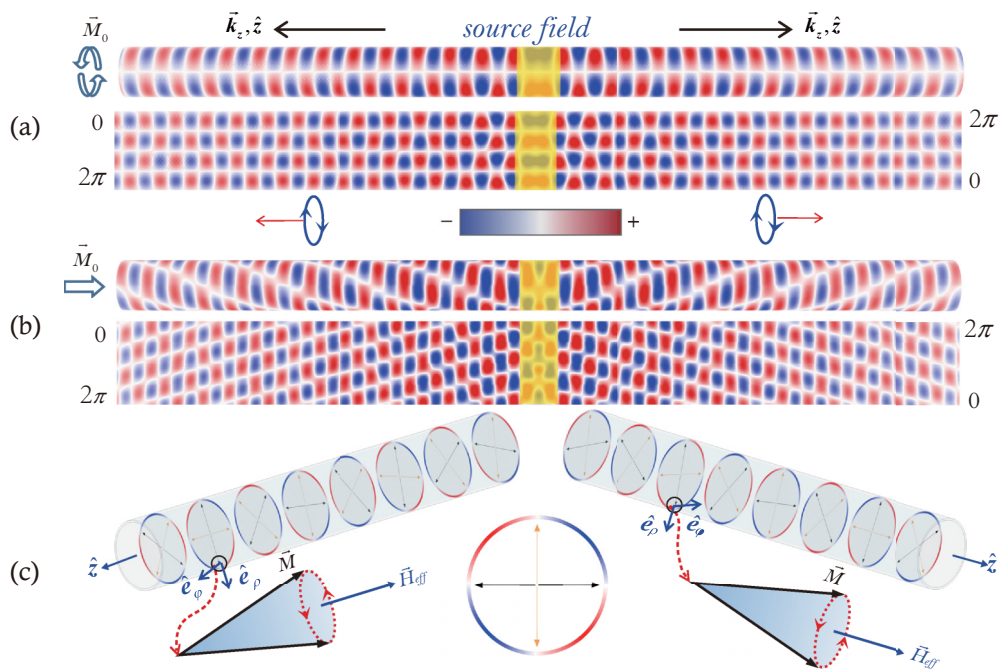


FIG. 1. (a) A snapshot of the dynamic radial component of the magnetization ( $\delta\vec{m}_r$ ) showing the profile of a 19 GHz mode ( $n = 2$ ) traveling in both directions of a circularly magnetized tube. Upper panel is the side view of the original tube while lower a rolled-out one. (b) Similar illustrations of a 19 GHz mode ( $n = 2$ ) in an axially magnetized tube. (c) Schematic drawings of a series of cross sections of the tube and the precession of local magnetization for the two SW branches propagating in opposite directions, respectively.

where  $\vec{m} = \frac{\vec{M}}{M_s}$  is the normalized magnetization,  $\gamma$  the gyromagnetic ratio,  $\vec{H}_{\text{eff}}$  the effective field,  $\alpha$  the Gilbert damping parameter, and  $M_s$  the saturation magnetization. We explore SW properties in ferromagnetic nanostructures by numerically solving the LLG equation, using a micromagnetic code MuMax3 [51]. Cylindrical nanowires with a diameter of 60 nm were exploited to serve as the SW waveguides. The material parameters used in our simulations are typical for Permalloy, with  $\mu_0 M_s = 1$  T, exchange constant  $A = 1.3 \times 10^{-11}$  J/m,  $\alpha = 0.01$ , and zero crystallographic anisotropy. We first address the SWs propagating in a hollow cylinder with a thickness of 2 nm. In such a thin tube, the radial distribution of the SWs can be ignored. Here we focus on modes that have nonuniform azimuthal distribution. Recalling the usual behavior of waves propagating in waveguides, one can easily anticipate the formation of a circular standing wave around the axis of the tube. Because of the natural boundary condition, the standing-wave wave vector must satisfy  $k_\phi = \frac{2n\pi}{L}$ , where  $L$  is the outer circumference of the tube and  $n$  a positive integer number. Such a mode with a particular frequency and a specific order (denoted by  $n$ ) can be excited in simulations by applying a local sinusoidal field with a proper azimuthal distribution, as shown in Fig. 1. Suppose the initial state of the wire is given by  $\vec{m}_0$ , the magnetization field after excitation can be written as  $\vec{m} = \vec{m}_0 + \delta\vec{m}$ , where  $\delta\vec{m}(\vec{r}, t)$  is the dynamic magnetization representing the SW mode profile. For comparison, we first consider SW modes of this type excited in a tube magnetized around its axis in equilibrium by applying a circulating field. In Fig. 1(a), the profile of a 2nd-order ( $n = 2$ ) mode is illustrated by showing a snapshot of the dynamic radial component of the magnetiza-

tion ( $\delta\vec{m}_r$ ) taken both from the side view of the original tube and a “rolled-out” one. It is clear that a regular standing-wave pattern is formed in the azimuthal direction as expected. The profile shown in the “rolled-out” tube looks essentially the same as those of SW modes propagating in a flat thin-film strip. Note that the left- and right-running SW branches shown in Fig. 1(a) actually differ slightly in wavelength, which is consistent with Refs. [21,23] (see Fig. s1 of the Supplemental Material [52] for other simulation results showing a more obvious SW nonreciprocity in a circularly magnetized tube).

We now turn to a different equilibrium configuration of the wire. Without an external field, the wire is naturally magnetized along its axial direction due to the shape anisotropy. Figure 1(b) displays the profile of a similarly excited 2nd-order mode propagating in an axially magnetized tube. Although a perfect standing-wave pattern is maintained in each cross section of the tube, the azimuthal positions of the (anti)nodes continue to shift during the wave propagation, showing an evident rotation around the axis. This behavior is more clearly depicted in a schematic plotting a series of cross sections (real data) in a transparent tube as shown in Fig. 1(b). For a guiding purpose, two diameters of each cross section connecting two next-neighboring nodes are drawn in dashed lines. A movie clearly showing the SW rotation can be found in the Supplemental Material [52]. As shown in Fig. 1, the oscillating field located in the middle of the wire excited two SW branches propagating in opposite directions. Note that they exhibit opposite senses of rotation. For the (right) left-running wave, the rotation appears to be (clockwise) counterclockwise while looking in the direction of the source. Adopting the terminology used in optical activity, the tube is therefore *d*

rotatory ( $l$  rotatory) when the wave propagation is parallel (antiparallel) to the equilibrium magnetization.

### III. DISCUSSIONS

The apparent likeness between this SW effect and the optical activity further extends to the physical model behind. Thinking of standing-wave generation and following the idea of Fresnel's treatment, the SW modes obtained in the simulations can also be considered to be constructed by the superposition of two constituent waves with the same frequency but different propagating speeds. Consequently, the spatial profiles of the dynamic components of magnetization,  $\delta\vec{m}_\rho$  and  $\delta\vec{m}_\phi$ , can be expressed by the following assumed formula,

$$\begin{aligned} \delta\vec{m}_j(\phi, z) &= \delta\vec{m}_{j0}[e^{i(\omega t+n\phi-k_{z1}z)} + e^{i(\omega t-n\phi-k_{z2}z)}] \\ &= 2\delta\vec{m}_{j0} \cos\left[n\left(\phi - \frac{k'_z}{n}z\right)\right] e^{i(\omega t-k''_z z)}, \quad j = \rho, \phi, \end{aligned} \quad (2)$$

where  $\delta\vec{m}_{j0}$  is a complex constant,  $\omega$  the angular frequency,  $n$  a positive integer number,  $k_{z1}$  and  $k_{z2}$  two wave vectors assumed to be different,  $k'_z = \frac{k_{z1}-k_{z2}}{2}$  and  $k''_z = \frac{k_{z1}+k_{z2}}{2}$ . We refer to the constituent wave with a factor  $e^{i(\omega t+n\phi-k_{z1}z)}$  as the  $\mathcal{R}$  state and  $e^{i(\omega t-n\phi-k_{z2}z)}$  the  $\mathcal{L}$  state, similar to the definitions in optics. Obviously, the formula in Eq. (2) well describes the feature of SW modes in the axially magnetized tube assuming different dispersion relation for the  $\mathcal{R}$  and  $\mathcal{L}$  states. We mention that the wave patterns obtained in simulations can

be perfectly reproduced by computer graphics using Eq. (2) (see Fig. s2 of the Supplemental Material [52]). In the case of  $k_{z1} = k_{z2}$ , the trivial mode profile observed in the circularly magnetized configuration is then retrieved.

In the following, we explain the physical mechanism causing the different dispersion of the  $\mathcal{R}$  and  $\mathcal{L}$  states in the longitudinal configuration. There are two interactions in the studied system that jointly govern the magnetization dynamics, namely, the Heisenberg exchange interaction and the dipolar interaction. The effective field  $\vec{H}_{\text{eff}}$  in Eq. (1) thus includes two terms, the exchange field  $\vec{h}_{\text{exc}}$  and the dipolar field  $\vec{h}_d$ . The former, given by  $\vec{h}_{\text{exc}} = D\nabla^2\vec{m}$ , where  $D = \frac{2A}{\mu_0 M_s}$ , certainly does not differentiate the two states. The latter has two sources, the surface and the volume magnetic charges generated in the magnetic sample. In a cylindrical coordinate system applicable for a tube, the volume charge density is given by  $\rho_v = -\nabla \cdot \vec{m} = -[\frac{\partial m_\rho}{\partial \rho} + \frac{1}{\rho} \frac{\partial m_\phi}{\partial \phi} + \frac{\partial m_z}{\partial z}]$ . For an axially magnetized thin tube ( $\vec{m}_0 = \hat{z}$ ,  $\delta\vec{m} \approx \delta\vec{m}_\rho \hat{\rho} + \delta\vec{m}_\phi \hat{\phi}$ ), one gets  $\rho_v = -\frac{1}{\rho}(\delta\vec{m}_\rho + \frac{\partial \delta\vec{m}_\phi}{\partial \phi})$ . For waves propagating in the right half of the tube as shown in Fig. 1 (the positive direction of the polar axis is always set to be parallel to the propagation), the precession of a local magnetic moment around the effective field is sketched. Considering the precessional direction determined by Eq. (1), the two dynamic components of an  $\mathcal{R}$  state ( $\mathcal{L}$  state) can thus be written as  $\delta\vec{m}_\rho = |\delta\vec{m}_{\rho 0}|e^{i(\omega t \pm n\phi - k_{z1(2)}z)}$ ,  $\delta\vec{m}_\phi = -i|\delta\vec{m}_{\phi 0}|e^{i(\omega t \pm n\phi - k_{z1(2)}z)}$ . The volume charge density for the  $\mathcal{R}$  state ( $\mathcal{L}$  state) is then given by  $\rho_v = -\frac{1}{\rho}(|\delta\vec{m}_{\rho 0}| \pm n|\delta\vec{m}_{\phi 0}|)e^{i(\omega t \pm n\phi - k_{z1(2)}z)}$ . Clearly, the  $\mathcal{R}$  state has a larger

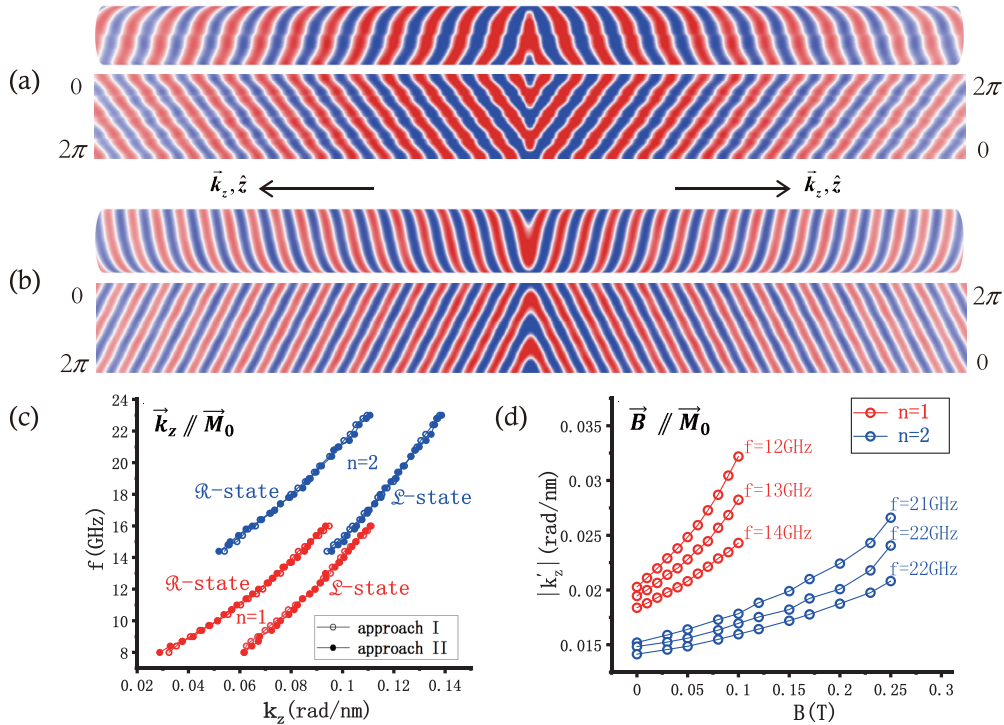


FIG. 2. (a) Profiles of a 19 GHz right-running  $\mathcal{R}$  state together with a left-running  $\mathcal{L}$  state. (b) Profiles of a 19 GHz right-running  $\mathcal{L}$  state together with a left-running  $\mathcal{R}$  state. (c) SW dispersion relations of the  $\mathcal{R}$  and  $\mathcal{L}$  states obtained in two approaches: direct measurement of the constituent modes (I) and extraction from the profile of the composite modes via the Fresnel model (II). (d) Dependence of the rotatory power of the tube on the field strength. Lines in (c) and (d) are only guides to the eye.

average charge density and consequently higher dipolar energy than the  $\mathcal{L}$  state. To have the same frequency, the total energy of the  $\mathcal{L}$  state must be compensated by having a larger exchange portion, meaning that  $k_{z2} > k_{z1}$ . Therefore, one has  $k'_z < 0$  in Eq. (2), yielding a  $d$ -rotatory mode composed of the  $\mathcal{R}$  and  $\mathcal{L}$  states. In contrast, for waves traveling in the left half of the tube with reversed polar axis and azimuthal direction, the relative phase difference between the two dynamic components  $\delta\bar{m}_\rho$  and  $\delta\bar{m}_\phi$  assumes a change of  $\pi$ . Consequently, an  $l$ -rotatory behavior is deduced by the same argument. For a circularly magnetized tube ( $\bar{m}_0 = \hat{\phi}$ ) with a negligible dynamic azimuthal component, the  $\mathcal{R}$  and  $\mathcal{L}$  states must share the same dispersion relation, giving  $k'_z = 0$  in Eq. (2).

After Fresnel proposed his phenomenological model for the optical activity, he successfully designed a composite prism allowing the separation of the two circular components of a linear light beam. In our simulations, the SW constituent  $\mathcal{R}$  and  $\mathcal{L}$  states can also be excited independently by applying a local field with its temporal and spatial distribution given by  $\cos(\omega t \pm n\phi)$ . Wave profiles of those two states with a degenerate frequency are shown in Figs. 2(a) and 2(b). Note that while exciting a right-running  $\mathcal{R}$  state ( $\mathcal{L}$  state), the source field simultaneously excites a left-running  $\mathcal{L}$  state ( $\mathcal{R}$  state). Evidently, the  $\mathcal{R}$  and  $\mathcal{L}$  states moving in the same direction have well-defined yet distinct wavelengths, assuring that they are eigenexcitations of the system yet with different propagating speeds. Besides this direct measurement, the dispersion relations of the  $\mathcal{R}$  and  $\mathcal{L}$  states can also be extracted from the profiles of the composite modes by calculating  $k'_z$  and  $k''_z$  in Eq. (2). A perfect match is obtained between those two approaches, as shown by the data plotted respectively in Fig. 2(c). Beside the sample size and material, the SW dispersion also depends on the external magnetic field applied to the wire, which hence can be conveniently exploited to tailor its rotatory power (characterized by  $k'_z$ ). The field dependencies of  $k'_z$  for various modes are obtained in simulations, some of which are plotted in Fig. 2(d). Here we make a quantitative comparison with the optical activity and the Faraday effect. To evaluate the field influence, one may define  $\nu = \frac{dk'_z}{dB}$ , which has the same dimension as the Verdet constant in the Faraday effect though being field dependent in this case. While the rotatory power and the Verdet constant for quartz, for instance, under usual circumstances are of the order of  $10^\circ/\text{mm}$  and  $10^{-2}$  min of arc  $\text{gauss}^{-1} \text{cm}^{-1}$ , respectively [1], they are roughly of the order of  $10^5^\circ/\text{mm}$  and  $10^4$  min of arc  $\text{gauss}^{-1} \text{cm}^{-1}$  or higher for the studied SWs and wires here.

Finally, we point out that the magnonic activity effect is also observed in solid nanocylinders. As illustrated in Fig. 3, a SW mode with a circular standing-wave pattern, obtained

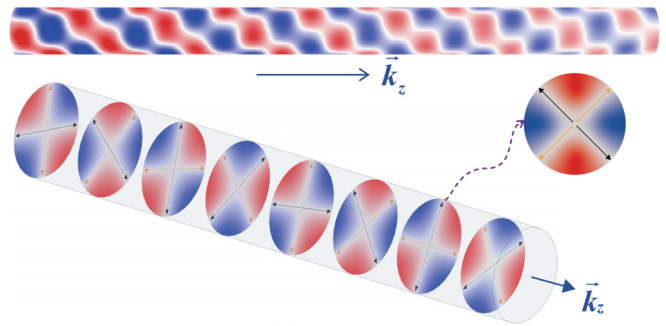


FIG. 3. Profile of a 35 GHz SW mode propagating in a 60 nm diameter solid wire magnetized in the axial direction. Both the surface and inside of the wire are shown.

in a 60 nm diameter solid wire magnetized along its axial direction, shows an alike rotation during its propagation. Such a mode is excited in the same way as in a tube by applying a local oscillating field with a nonuniform azimuthal distribution. In principle, the SW modes in a solid wire can also have a radial distribution [43], which further complicates the calculation of the dynamical volume charges. Nevertheless, the SW chirality of the  $\mathcal{R}$  and  $\mathcal{L}$  states, which originates from the azimuthal contribution of the volume charges, remains in a solid wire. Therefore, a cylindrical nanowire, either hollow or solid, is magnonically active due to its overall curvilinear shape.

#### IV. SUMMARY

In summary, we describe a magnonic version of the optical activity, predicting the existence of chiral SWs, i.e., circular SW modes that distinguish handedness. Quantitatively, the SW chiral effect in ferromagnetic nanocylinders is much more significant compared to that of optically active materials in terms of rotatory power and field sensitivity. The recent technical progress in fabrication and measurement of 3D magnetic nanostructures [24,26,36,37,39,41,44,45] may pave the way for future experimental explorations of relevant effects, which present new aspects for SW manipulations, essential to the development of novel spintronic devices based on SW propagations.

#### ACKNOWLEDGMENTS

This work is supported by the National Natural Science Foundation of China (Grant No. 11774218) and Shanghai Key Laboratory of High Temperature Superconductors (Grant No. 14DZ2260700).

- [1] E. Hecht, *Optics* (Addison Wesley, San Francisco, CA, 2002).
- [2] L. Pasteur, *Ann. Chim. Phys. Sér. 3* **24**, 442 (1848).
- [3] L. D. Barron, *Chem. Soc. Rev.* **15**, 189 (1986).
- [4] M. Quack, *Angew. Chem. Int. Ed. Engl.* **28**, 571 (1989).
- [5] A. Khitun, M. Bao, and K. L. Wang, *J. Phys. D* **43**, 264005 (2010).

- [6] A. A. Serga, A. V. Chumak, and B. Hillebrands, *J. Phys. D* **43**, 264002 (2010).
- [7] B. Lenk, H. Ulrichs, F. Garbs, and M. Münzenberg, *Phys. Rep.* **507**, 107 (2011).
- [8] M. Krawczyk and D. Grundler, *J. Phys.: Condens. Matter* **26**, 123202 (2014).

- [9] A. V. Chumak, V. I. Vasyuchka, A. A. Serga, and B. Hillebrands, *Nat. Phys.* **11**, 453 (2015).
- [10] J. M. Owens, J. H. Collins, and R. L. Carter, *Circuits Syst. Signal Process.* **4**, 317 (1985).
- [11] J. D. Adam, *Proc. IEEE* **76**, 159 (1988).
- [12] A. V. Chumak, A. A. Serga, and B. Hillebrands, *Nat. Commun.* **5**, 4700 (2014).
- [13] K. Vogt, *Nat. Commun.* **5**, 3727 (2014).
- [14] R. Streubel, P. Fischer, F. Kronast, V. P. Kravchuk, D. D. Sheka, Y. Gaididei, O. G. Schmidt, and D. Makarov, *J. Phys. D: Appl. Phys.* **49**, 363001 (2016).
- [15] A. Fernández-Pacheco, R. Streubel, O. Fruchart, R. Hertel, P. Fischer, and R. P. Cowburn, *Nat. Commun.* **8**, 15756 (2017).
- [16] M. Yan, A. Kákay, S. Gliga, and R. Hertel, *Phys. Rev. Lett.* **104**, 057201 (2010).
- [17] M. Yan, C. Andreas, A. Kákay, F. Garcia-Sanchez, and R. Hertel, *Appl. Phys. Lett.* **99**, 122505 (2011).
- [18] M. Yan, C. Andreas, A. Kákay, F. Garcia-Sanchez, and R. Hertel, *Appl. Phys. Lett.* **100**, 252401 (2012).
- [19] J. Otálora, J. López-López, P. Vargas, and P. Landeros, *Appl. Phys. Lett.* **100**, 072407 (2012).
- [20] O. V. Pylypovskiy, V. P. Kravchuk, D. D. Sheka, D. Makarov, O. G. Schmidt, and Y. Gaididei, *Phys. Rev. Lett.* **114**, 197204 (2015).
- [21] J. A. Otálora, M. Yan, H. Schultheiss, R. Hertel, and A. Kákay, *Phys. Rev. Lett.* **117**, 227203 (2016).
- [22] S. Vojkovic, V. L. Carvalho-Santos, J. M. Fonseca, and A. S. Nunez, *J. Appl. Phys.* **121**, 113906 (2017).
- [23] J. A. Otálora, M. Yan, H. Schultheiss, R. Hertel, and A. Kákay, *Phys. Rev. B* **95**, 184415 (2017).
- [24] M. Wyss *et al.*, *Phys. Rev. B* **96**, 024423 (2017).
- [25] J. Yang, J. Kim, B. Kim, Y.-J. Cho, J.-H. Lee, and S.-K. Kim, *J. Appl. Phys.* **123**, 033901 (2018).
- [26] M. Zimmermann *et al.*, *Nano Lett.* **18**, 2828 (2018).
- [27] O. V. Pylypovskiy, D. Makarov, V. P. Kravchuk, Y. Gaididei, A. Saxena, and D. D. Sheka, *Phys. Rev. Appl.* **10**, 064057 (2018).
- [28] J. A. Otálora, A. Kákay, J. Lindner, H. Schultheiss, A. Thomas, J. Fassbender, and K. Nielsch, *Phys. Rev. B* **98**, 014403 (2018).
- [29] O. M. Volkov, D. D. Sheka, Y. Gaididei, V. P. Kravchuk, U. K. Röbber, J. Fassbender, and D. Makarov, *Sci. Rep.* **8**, 866 (2018).
- [30] X. Huo and Y. Liu, *New J. Phys.* **21**, 093024 (2019).
- [31] J. Rychlý, V. S. Tkachenko, J. W. Klos, A. Kuchko, and M. Krawczyk, *J. Phys. D: Appl. Phys.* **52**, 075003 (2019).
- [32] M. C. Depassier, *Phys. Rev. B* **100**, 144402 (2019).
- [33] M. Mohseni, R. Verba, T. Brächer, Q. Wang, D. A. Bozhko, B. Hillebrands, and P. Pirro, *Phys. Rev. Lett.* **122**, 197201 (2019).
- [34] M. Schöbitz, A. De Riz, S. Martin, S. Bochmann, C. Thirion, J. Vogel, M. Foerster, L. Aballe, T. O. Menteş, A. Locatelli, F. Genuzio, S. Le-Denmat, L. Cagnon, J. C. Toussaint, D. Gusakova, J. Bachmann, and O. Fruchart, *Phys. Rev. Lett.* **123**, 217201 (2019).
- [35] C. Jia, D. Ma, A. F. Schäffer, and J. Berakdar, *Nat. Commun.* **10**, 2077 (2019).
- [36] O. M. Volkov, A. Kákay, F. Kronast, I. Mönch, M.-A. Mawass, J. Fassbender, and D. Makarov, *Phys. Rev. Lett.* **123**, 077201 (2019).
- [37] O. M. Volkov, F. Kronast, I. Mönch, M. Mawass, A. Kákay, J. Fassbender, and D. Makarov, *Phys. Status Solidi RRL* **13**, 1800309 (2019).
- [38] M. C. Giordano, K. Baumgaertl, S. E. Steinvall, J. Gay, M. Vuichard, A. F. Morral, and D. Grundler, *ACS Appl. Mater. Interfaces* **12**, 40443 (2020).
- [39] C. Phatak, C. S. Miller, Z. Thompson, E. B. Gulsoy, and A. K. Petford-Long, *ACS Appl. Nano Mater.* **3**, 6009 (2020).
- [40] A. Pavlis and C. Psaroudaki, *Phys. Rev. Research* **2**, 032058(R) (2020).
- [41] C. Donnelly and V. Scagnoli, *J. Phys.: Condens. Matter* **32**, 213001 (2020).
- [42] D. Mancilla-Almonacid, M. A. Castro, J. M. Fonseca, D. Altbir, S. Allende, and V. L. Carvalho-Santos, *J. Magn. Magn. Mater.* **507**, 166754 (2020).
- [43] Y. Jiang, H. Y. Yuan, Z.-X. Li, Z. Wang, H. W. Zhang, Y. Cao, and P. Yan, *Phys. Rev. Lett.* **124**, 217204 (2020).
- [44] J. Llandro *et al.*, *Nano Lett.* **20**, 3642 (2020).
- [45] A. Fernández-Pacheco, L. Skoric, J. M. De Teresa, J. Pablo-Navarro, M. Huth, and O. V. Dobrovolskiy, *Materials* **13**, 3774 (2020).
- [46] H. D. Salinas, J. Restrepo, and Ó. Iglesias, *Phys. Rev. B* **101**, 054419 (2020).
- [47] V. L. Carvalho-Santos, R. M. Corona, D. Altbir, and S. Castillo-Sepúlveda, *Phys. Rev. B* **102**, 024444 (2020).
- [48] P. Ansalone and V. Basso, *Physica B* **578**, 411872 (2020).
- [49] D. D. Sheka, O. V. Pylypovskiy, P. Landeros, Y. Gaididei, A. Kákay, and D. Makarov, *Commun. Phys.* **3**, 128 (2020).
- [50] D. Kechrakos, L. Tzannetou, and A. Patsopoulos, *Phys. Rev. B* **102**, 054439 (2020).
- [51] A. Vansteenkiste and B. Van de Wiele, *J. Magn. Magn. Mater.* **323**, 2585 (2011).
- [52] See Supplemental Material at <http://link.aps.org/supplemental/10.1103/PhysRevB.103.094404> for a movie showing the circular standing-wave pattern formed in each cross section of the tube and its rotation during the wave propagation.